Proton Scattering by Isobars and Single Isotopes

J. BENVENISTE AND A. C. MITCHELL
Lawrence Radiation Laboratory, University of California, Livermore, California

AND

B. BUCK* AND C. B. FULMER
Oak Ridge National Laboratory,† Oak Ridge, Tennessee

(Received 5 August 1963)

Differential cross sections for proton inelastic scattering to the first excited (2+) states of Fe^{56}, Fe^{58}, Ni^{68}, Ni^{64}, and Zn^{64} are reported for bombarding energies near 10 MeV. Elastic- and inelastic-scattering angular distribution data were analyzed by a recently reported generalization of the optical model in which states of quadrupole collective motion strongly coupled to the nuclear ground state are considered. The results of this analysis show a dependence of the real nuclear potential depth on the nuclear symmetry parameter $(N-Z)/A$; the symmetry term for the real potential was found to be $\sim[23(N-Z)/A]$ MeV.

IT is well known that the nuclear optical model has been used very successfully in describing experimental proton-nucleus elastic-scattering data for a large range of proton energies and over a large breadth of nuclear mass. The most extensively used formulation of the optical model has employed spherically symmetric potentials. Recently a generalization of the optical model was reported[1] in which states of quadrupole collective motion strongly coupled to the nuclear ground state were considered. The model was used to analyze experimental data obtained by scattering protons from Ti, Cr, Fe, Ni, and Zn; angular distributions of both elastic and inelastic scattering to low-lying excited states were calculated. Good agreement between experimental and theoretical results was obtained.

In previously reported experiments[2,3] proton elastic scattering angular distributions of Fe^{56}, Fe^{58}, Ni^{58}, Ni^{64}, and Zn^{64} were obtained at energies near 10 MeV. These data were examined in terms of the results of extensive optical-model analyses of other data in which spherically symmetric potentials were used. This study yielded experimental evidence of a dependence of the real nuclear potential well depth on the nuclear symmetry parameter, $(N-Z)/A$.

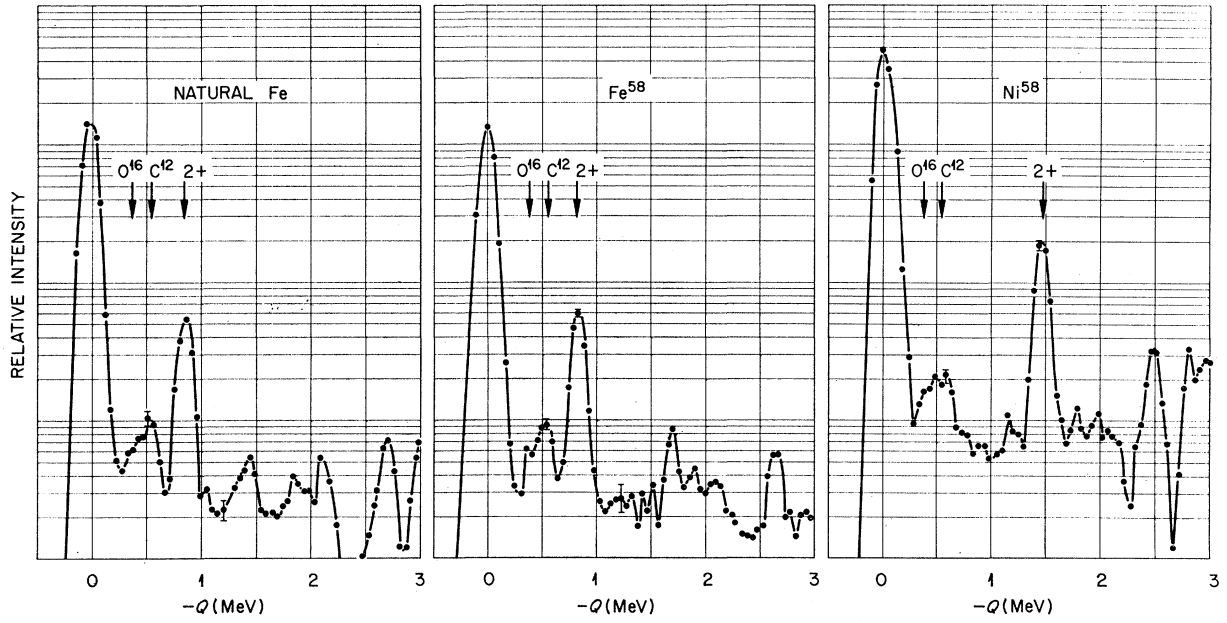

FIG. 1. Energy spectra of scattered protons from Fe^{56}, Fe^{58}, and Ni^{58}. The incident proton energy was 11.66 MeV and the detection angle was 50 deg. Zero abscissa corresponds to elastically scattered protons. The double peaks between $-Q=0.3$ and 0.65 MeV are due to oxygen and carbon impurities.

* Present address is Oxford University, Oxford, England.
† Operated for the U. S. Atomic Energy Commission by Union Carbide Corporation.
[1] B. Buck, Phys. Rev. **130**, 712 (1963).
[2] J. Benveniste, A. C. Mitchell, and C. B. Fulmer, Phys. Rev. **129**, 2173 (1963).
[3] J. Benveniste, A. C. Mitchell, and C. B. Fulmer, preceding paper, Phys. Rev. **135**, B317 (1964).

TABLE I. Maximum impurity correction for target foils used in the work reported here. Exact value of the correction depends on the angle.

Target	Impurity corrections		
	C^{12} (%)	O^{16} (%)	Angular region (deg)
Fe^{56}	<12	<25	60–85
Fe^{58}	< 3	<15	60–85
Ni^{58}	<10	<13	85–130
Ni^{64}	<50	<30	80–115
Zn^{64}	<34	<36	65–95

Angular distributions of the inelastic scattering to the first excited (2+) states of the targets studied in Refs. 2 and 3 have been extracted from experimental data. It is the purpose of this paper to report these data and the results of an analysis in which the generalized optical model discussed in Ref. 1 was used to calculate simultaneously both the elastic- and inelastic-scattering angular distributions. This extends the number of nuclei used to test the model and includes analyses of data obtained from isobars, a feature that was not included in Ref. 1. The role of the nuclear symmetry parameter is thus examined in terms of the generalized optical model.

The experimental data were obtained with the external proton beam of the variable-energy cyclotron of the Lawrence Radiation Laboratory at Livermore. A detailed description of the experiment is given in Ref. 2. An important feature of the experiment, especially for the inelastic-scattering data, is that a particle identifica-

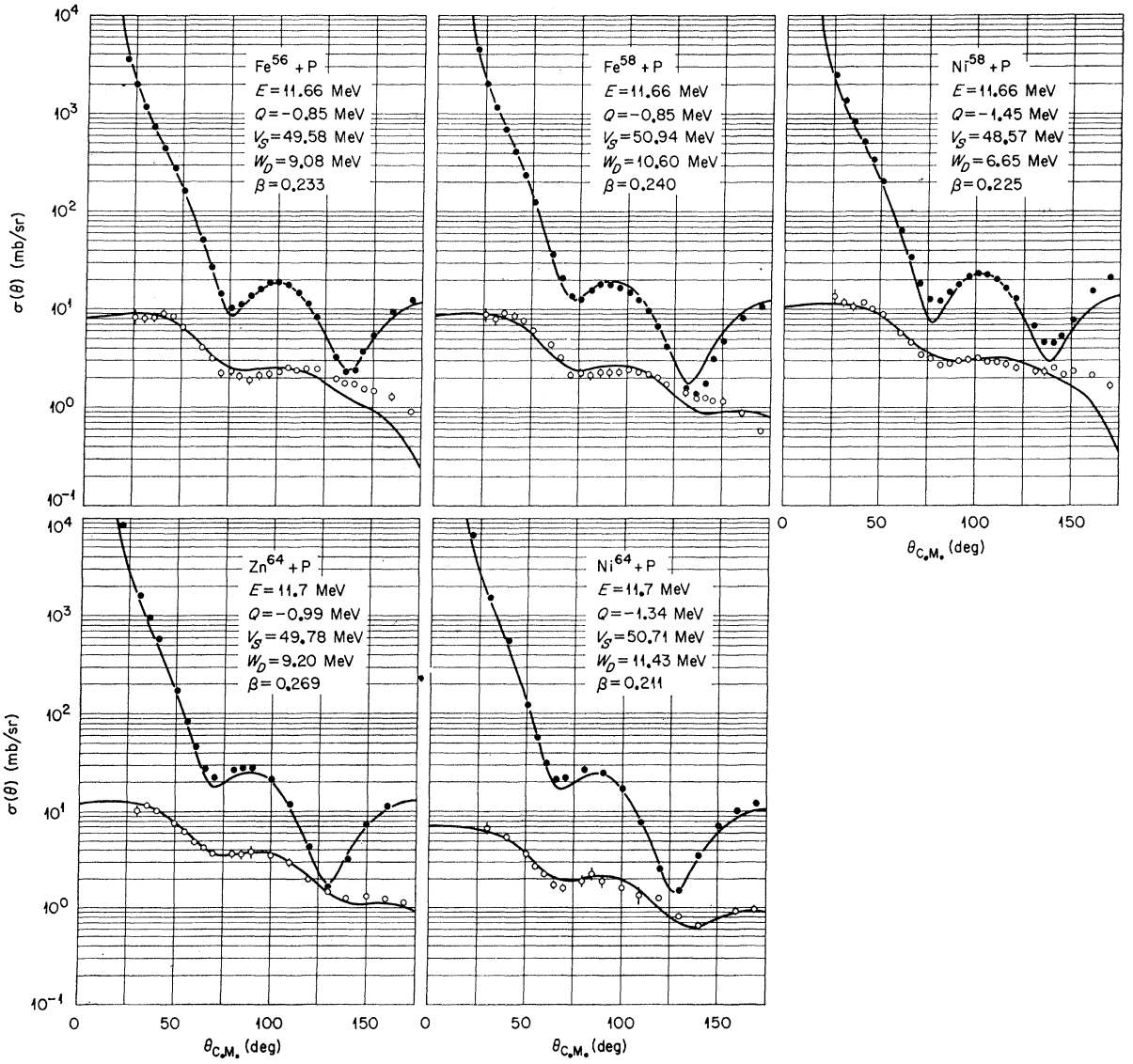

FIG. 2. Comparison of experimental and theoretical results at E_p=11.7 MeV. The solid curves are theoretical; the solid points are experimental elastic-scattering data and the open circles are experimental inelastic-scattering data. Error flags are shown for experimental inelastic-scattering data where the uncertainties are ≥5%.

TABLE II. Differential cross sections for inelastic scattering to first excited state.

E_p=10.93 MeV			E_p=11.66 MeV		
θ c.m. (deg)	$\sigma(\theta)$ (mb/sr)	±%	θ c.m. (deg)	$\sigma(\theta)$ (mb/sr)	±%
			Fe^{56}		
30.7	6.8	13	25.6	8.3	15
35.6	7.6	16	30.6	8.1	10
40.7	9.0	7	35.7	8.2	10
50.8	8.1	7	40.7	8.9	5
60.9	5.2	6	45.8	8.4	4
65.9	3.5	7	50.8	6.5	4
71.0	3.1	12	60.9	4.0	4
76.0	2.4	12	65.9	3.17	4
81.0	2.7	12	71.0	2.25	6
86.0	2.5	12	76.0	2.35	8
91.0	2.9	12	81.0	2.08	8
96.0	2.8	8	86.0	1.90	8
101.0	3.1	5	91.0	2.11	8
106.0	2.6	7	96.0	2.20	8
111.0	3.0	7	100.9	2.30	4
120.9	2.4	5	105.9	2.49	4
125.8	2.8	6	110.8	2.41	4
130.8	2.2	6	115.8	2.42	4
135.7	1.8	7	120.7	2.42	4
140.7	1.8	7	130.6	1.98	4
150.5	1.5	7	135.5	1.78	4
160.4	1.5	8	140.4	1.77	4
170.2	1.4	8	144.9	1.54	4
			150.3	1.47	4
			160.3	1.30	6
			169.9	0.90	7
E_p=10.93 MeV			E_p=11.66 MeV		
			Fe^{58}		
30.5	7.36	16	25.6	8.9	15
35.6	8.32	9	30.6	8.1	10
40.7	8.72	6	35.7	9.1	8
50.8	6.32	8	40.7	8.7	6
60.9	4.45	5	45.8	7.8	4
65.9	2.75	6	50.8	6.1	4
71.0	2.55	6	60.9	4.4	4
76.0	1.97	12	65.9	3.30	4
81.0	2.39	12	71.0	2.16	5
86.0	2.47	12	76.0	2.30	7
91.0	2.12	12	81.0	2.11	7
96.0	2.54	6	86.0	2.28	7
101.0	2.63	6	91.0	2.28	7
106.0	2.36	7	96.0	2.30	7
111.0	2.25	6	100.9	2.44	4
120.9	1.89	7	105.9	2.31	4
125.8	1.82	7	110.8	2.13	4
130.8	1.58	5	115.8	2.00	4
135.7	1.17	7	120.7	1.67	4
140.7	1.23	7	130.6	1.40	5
150.5	1.14	7	135.5	1.25	5
160.4	0.715	8	140.4	1.22	5
170.2	0.482	10	144.9	1.15	4
			150.3	1.13	5
			160.3	0.88	5
			169.9	0.57	6
E_p=10.88 MeV			E_p=11.66 MeV		
			Ni^{58}		
30.5	9.9	6	25.6	13.3	15
35.6	8.5	12	30.6	12.2	8
40.7	9.5	4	35.7	10.5	8
50.8	8.8	4	40.7	11.3	5
60.9	6.1	4	45.8	9.7	4
65.9	4.9	7	50.8	8.8	4
71.0	4.6	4	60.9	5.66	4
76.0	3.5	7	65.9	4.58	4

E_p=10.88 MeV			E_p=11.66 MeV		
θ c.m. (deg)	$\sigma(\theta)$ (mb/sr)	±%	θ c.m. (deg)	$\sigma(\theta)$ (mb/sr)	±%
			Ni^{58}		
81.1	3.3	4	71.0	3.38	4
86.1	3.2	7	76.0	3.11	4
91.1	3.2	4	81.0	2.66	4
96.1	3.0	8	86.0	2.76	4
101.1	3.3	4	91.0	2.89	5
106.0	3.0	5	96.0	3.02	5
110.0	2.8	5	100.9	3.15	4
120.9	3.0	5	105.9	2.88	4
125.8	2.3	5	110.8	2.83	4
130.8	2.3	5	115.8	2.70	6
135.7	2.4	6	120.7	2.50	6
140.7	2.5	5	130.6	2.29	5
150.5	2.6	5	135.5	2.38	5
160.4	2.7	5	140.4	2.51	4
170.2	2.9	5	144.9	2.18	4
			150.3	2.30	4
			160.3	2.08	4
			169.9	1.69	5
E_p=9.60 MeV			E_p=11.7 MeV		
			Ni^{64}		
30.5	5.4	8	30.5	6.66	12
35.6	6.03	8	40.6	5.49	5
40.6	5.31	5	50.7	3.60	5
50.7	3.69	5	55.8	2.70	5
60.8	2.52	5	60.8	2.25	5
65.9	2.07	6	65.9	1.71	6
70.9	1.89	4	70.9	1.62	6
75.9	1.80	6	80.9	1.89	10
80.9	1.89	4	85.9	2.25	15
91.0	2.25	20	90.0	1.89	15
96.0	1.89	20	100.9	1.62	15
100.9	1.89	20	110.9	1.35	20
110.8	1.35	25	120.8	1.26	4
120.8	1.53	25	130.7	0.81	4
125.8	1.17	40	140.6	0.64	5
130.7	1.08	15			
135.9	0.84	20	160.3	0.93	5
140.6	0.79	15	170.2	0.99	5
150.5	0.64	8			
160.3	0.58	8			
E_p=9.60 MeV			E_p=11.7 MeV		
			Zn^{64}		
25.4	8.64	15	30.5	10.1	10
30.5	10.8	6	35.5	11.4	5
35.6	10.0	6	40.6	11.1	4
40.6	10.6	4	50.7	7.74	4
50.7	8.37	4	55.8	6.12	4
60.8	5.67	3	60.8	4.86	4
65.9	4.50	5	65.9	4.14	4
70.9	3.78	4	70.9	3.60	5
75.9	4.05	5	80.9	3.60	10
80.9	3.15	7	85.9	3.60	10
91.0	3.42	10	90.9	3.78	15
96.0	2.34	20	100.9	3.51	8
100.9	3.60	20	110.9	2.88	8
110.8	2.70	25	120.8	1.98	4
120.8	2.25	25	130.7	1.53	4
125.8	1.80	25	140.6	1.26	5
130.7	2.61	5	150.5	1.35	5
135.7	2.25	5	160.3	1.26	5
140.6	1.98	5	170.2	1.17	5
150.5	1.53	5			
160.3	1.35	5			
170.2	1.17	5			

TABLE III. Optical-model parameters used in the analysis.

Parameter	Value
V_S	Variable
r_S	1.25 F
a_S	0.65 F
W_I	0.0 MeV
r_I	1.25 F
a_I	0.65 F
W_D	Variable
r_D	1.25 F
a_D	0.47 F
r_F	1.25 F
a_F	0.65 F
β	Variable
$V_{22}^{(2)}$	0.0 MeV
V_{SO}	8.00 MeV

tion system was used to ensure that the observed pulse-height spectra contain contributions due only to protons.

The energy spread of the incident beam was ~80 keV. For the Fe^{56} and Fe^{58} data and the 11.7-MeV Ni^{58} data the energy spread of the incident channel (ΔE of the target combined with ΔE of the beam) was ~100 keV; for the 10.9-MeV Ni^{58} data and the Ni^{64} and Zn^{64} data the energy spread of the incident channel was ~150 keV.

Typical spectra are shown in Fig. 1 for Fe^{56}, Fe^{58}, Ni^{58}; these are similar to the spectra for Ni^{64} and Zn^{64} given in Ref. 4. For Fig. 1 the raw pulse-height data were transformed to corrected energy spectra by the aid of a program called NEWDAC[5] and an IBM-7090 computer. The abscissa of a given peak corresponds to the excitation energy of that level. The excitation energy of the first 2+ level is indicated for each target. In each of the spectra there is a small peak at $-Q$~1.8 MeV about 10^{-3} as intense as the elastic scattering peak. This peak is attributed to inelastic scattering to the 1.78-MeV level of Si^{28} in the detector; the gamma ray escapes and thus the pulse height is reduced by 1.78 MeV.[6]

In the spectra of Fig. 1 the peaks due to the first excited states are clearly resolved. Peaks due to elastic scattering of protons from carbon and oxygen impurities in the target foils are also observed. In certain angular regions the kinematics of the systems resulted in the impurity peaks overlapping the peaks of interest. In the determination of inelastic-scattering cross sections corrections were made for the carbon and oxygen impurities and for isotopic impurities in the target foils.

TABLE IV. Comparison of theoretical and experimental cross sections for inelastic scattering to the first excited state.

Energy (MeV)	Target	σ_{In}^{2+} Experimental (mb)	σ_{In}^{2+} Theoretical (mb)
9.60	Ni^{64}	28.9	29.4
9.60	Zn^{64}	55.0	65.7
10.93	Fe^{56}	47.8	52.4
10.93	Fe^{58}	41.4	43.6
10.88	Ni^{58}	58.0	···
11.66	Fe^{56}	44.3	44.7
11.66	Fe^{58}	41.4	43.6
11.66	Ni^{58}	60.3	59.7
11.7	Ni^{65}	29.0	30.3
11.7	Zn^{64}	54.3	58.2

To facilitate making corrections for the carbon and oxygen impurities spectra of scattered protons from a Mylar target were obtained at each angle and angular distributions of elastic scattering from carbon and oxygen were thus determined. In the angular regions where the impurity peaks are clearly visible a normalization was made to the observations from the Mylar target. Thus by interpolating in the angular regions of overlap the correction for the impurities could be made rather well. Table I summarizes information on the impurity peak overlap region and the magnitude of the corrections for the various targets.

The correction for the presence of other isotopes was necessary only for the iron targets. For the inelastic scattering only Fe^{56} and Fe^{58} have levels that overlap within the energy resolution (~1%) of the experiment; thus

$$\sigma^1(Fe^{58}) = 0.784\sigma(Fe^{58}) + 0.187\sigma(Fe^{56}),$$
$$\sigma^1(Fe^{N}) = 0.003\sigma(Fe^{58}) + 0.919\sigma(Fe^{56}).$$

The numerical coefficients are fractional abundances of the isotopes in the targets that were used. These two equations were solved to yield the cross sections for transitions to the first excited states in terms of the σ^1 values which were measured experimentally. The uncertainties that were introduced by the necessity of these corrections are included in the errors shown in the tabulated cross sections in Table II.

The experimental inelastic-scattering cross sections are given in Table II. The indicated errors include contributions from statistics, beam-current integration measurements, geometrical factors, and uncertainties that resulted from target impurities. The experimental elastic-scattering cross sections are presented in tabular form in Refs. 2 and 3.

Figures 2 and 3 are graphical presentations of the elastic- and inelastic-scattering angular distributions for the several target nuclei studied. The experimental data are shown as individual points and the theoretical angular distributions are represented by the solid curves.

Details of the optical-model calculation are given in Ref. 1. The parameters by which the model was defined are given in Table III; the symbols for the parameters are in the notation that was used in Ref. 1. The parameters V_S, W_D, and β were varied in the calculation; the best fit values are listed on graphs in Figs. 2 and 3. These graphs show rather good agreement between the experimental and theoretical elastic-scattering angular distributions. The largest discrepancies are at large angles in the 9.6-MeV Zn^{64} and 11.66-MeV Ni^{58} angular distributions. The (p,n) threshold for Zn^{64} is 7.8 MeV and for Ni^{58} it is 9.3 MeV. Thus, experimental data in these two

[4] J. Benveniste, A. C. Mitchell, and C. B. Fulmer, Phys. Rev. 130, 309 (1963).
[5] J. B. Ball, ORNL Rept. 3405 (unpublished).
[6] J. Benveniste, A. C. Mitchell, and C. B. Fulmer, Phys. Rev. (to be published).

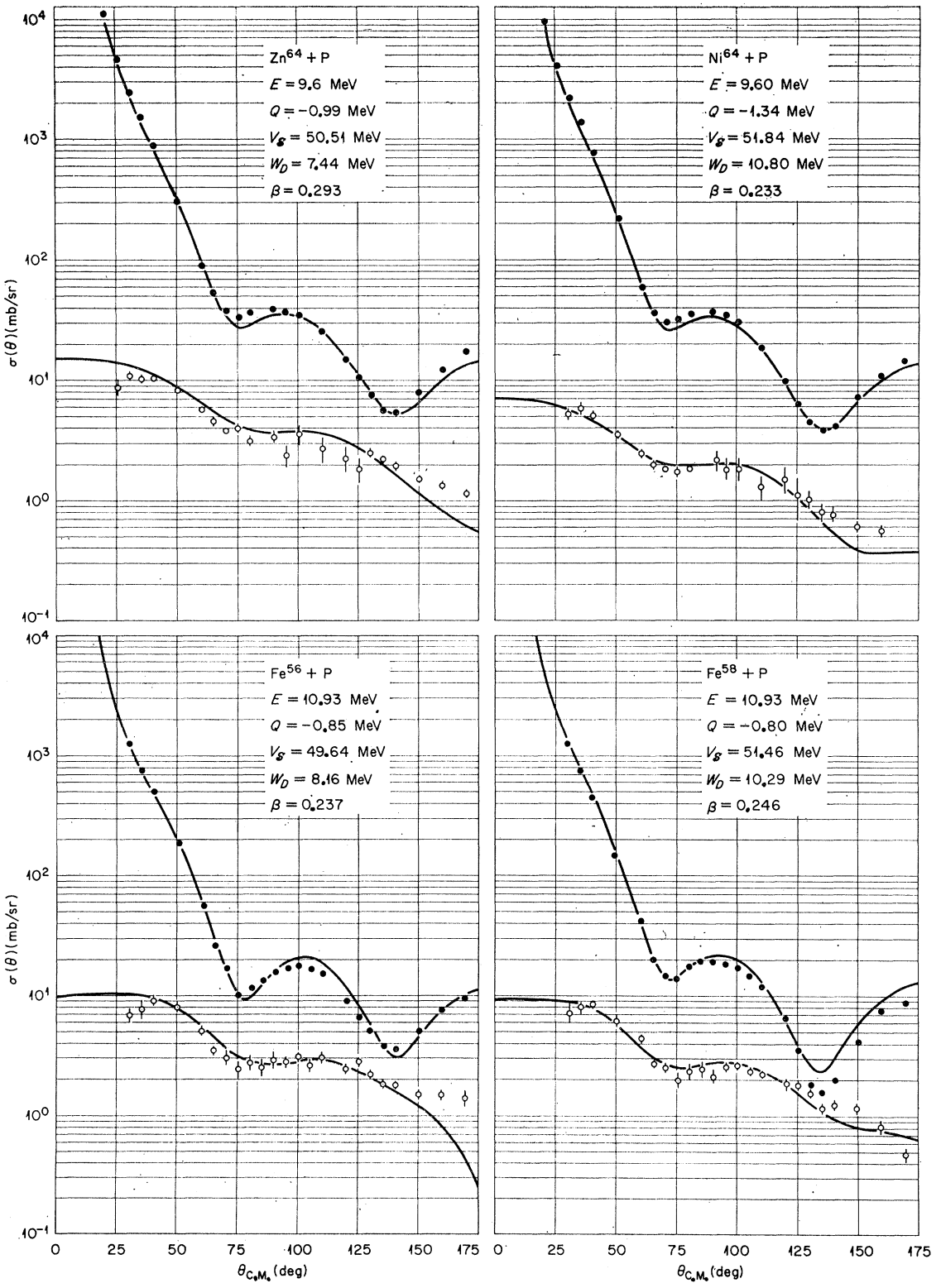

FIG. 3. Comparison of experimental and theoretical results at 9.6 and 10.9 MeV. The solid curves are theoretical; the solid points are experimental elastic-scattering data and the open circles are experimental inelastic-scattering data. Error flags are shown for experimental inelastic-scattering data where the uncertainties are $\geq 5\%$.

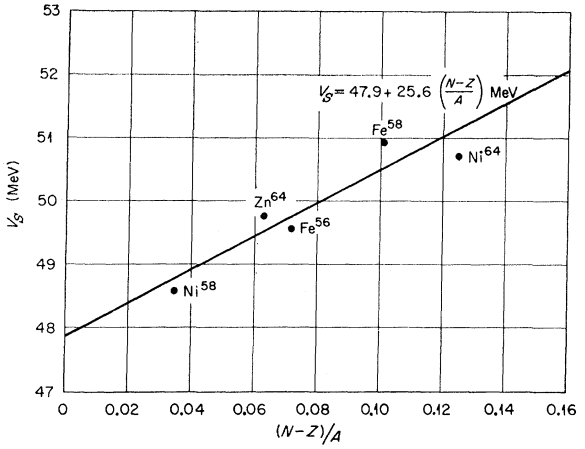

FIG. 4. Best-fit values of V_S versus $(N-Z)/A$ for data obtained at ~11.7 MeV. The straight line is a least-squares fit to the plotted points.

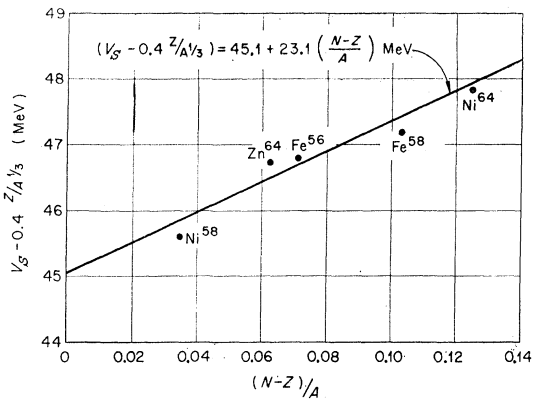

FIG. 5. Best-fit values of (V_S—Coulomb correction) versus $(N-Z)/A$ for data obtained at 11.7 MeV. The straight line is a least-squares fit to the plotted points.

cases include contributions from compound elastic scattering; this is most apparent at large angles where the shape elastic scattering is small. The compound-nucleus contributions to the 10.93-MeV Ni^{58} data were so large, especially in the inelastic data, that an optical-model fit was not attempted. The experimental inelastic-scattering cross sections include large uncertainties and large fluctuations between neighboring data points but the agreement between experimental and theoretical angular distributions is rather good, both in shape and absolute magnitude. The experimental and theoretical total inelastic-scattering cross sections are compared in Table IV. Compound-nucleus contributions qualitatively explain the large differences at large angles in the case of Ni^{58} at 11.6 MeV and Zn^{64} at 9.6 MeV.

In the calculations, the magnitudes of the deformation parameter, β, are determined mainly by the absolute normalization of the inelastic-scattering angular distributions. The values obtained from the analysis of the present data are compared in Table V with values of β that were determined from Coulomb excitation data.[7]

TABLE V. Comparison of deformation parameters obtained from proton scattering analysis and from Coulomb excitation data (Ref. 7).

Bombarding energy (MeV)	Nucleus	β (Proton scattering)	β (Coulomb excitation)
9.6	Ni^{64}	0.233	0.19
9.6	Zn^{64}	0.293	0.25
10.93	Fe^{56}	0.237	0.24
10.93	Fe^{58}	0.246	0.25
11.66	Fe^{56}	0.233	0.24
11.66	Fe^{58}	0.240	0.25
11.66	Ni^{58}	0.225	0.19
11.7	Ni^{64}	0.211	0.19
11.7	Zn^{64}	0.269	0.25

[7] P. H. Stelson (private communication; to be published).

The deformation parameter is defined by the expression

$$\beta^2 = B(E2:0 \rightarrow 2)/(\tfrac{3}{4}\pi Z e R_c^2)^2.$$

Good agreement is obtained for the β values for the iron isotopes. The large values from the proton scattering analysis of Ni^{58} and Zn^{64} data can be attributed to compound-nucleus contributions; in the case of Zn^{64} the value is substantially smaller for the 11.7-MeV data than for the 9.6-MeV data. The disagreement in the values of β obtained for Ni^{64} is not understood.

In a recent optical-model analysis (with spherically symmetric potentials) of proton elastic scattering in the range of[8] 9 to 22 MeV the observed increase of the real well depth as a function of mass number of the target nucleus was explained in part by a nuclear symmetry term in the potential, i.e., $V = V_0 + [(N-Z)/A]V_1$. In that work the value of V_1 was found to be 27 MeV. A

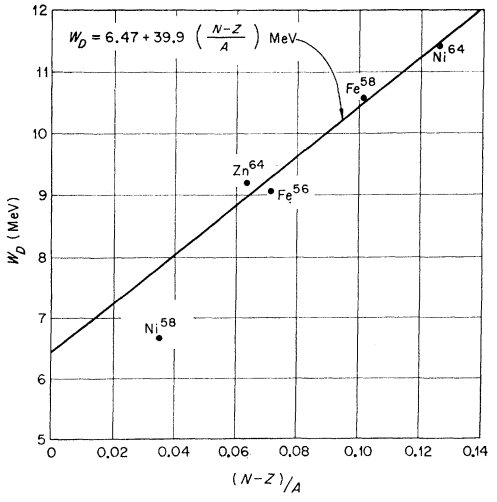

FIG. 6. Best-fit values of W_D versus $(N-Z)/A$ for data obtained at ~11.7 MeV. The solid line is a least-squares fit to the plotted points, with the Ni^{58} point not included.

[8] F. Perey, Phys. Rev. **131**, 745 (1963).

recent summary[9] of the various estimates shows a range from 16 to 50 MeV. A plot of the best-fit values of V_S versus $(N-Z)/A$ for our 11.7-MeV data is shown in Fig. 4. The solid line is the straight-line least-squares fit to the plotted points.

It is more realistic to apply a correction for the Coulomb potential before extracting the nuclear symmetry dependence of the potential. After careful consideration, the author of Ref. 8 took the Coulomb correction to be $0.4\,Z/A^{1/3}$ MeV. This correction was applied to the best-fit values of V_S for the 11.7-MeV data; the results are plotted in Fig. 5. These results, which were obtained from a generalized optical-model analysis, show definite evidence for a nuclear symmetry dependence of the real nuclear potential. The magnitude of V_1, as indicated by this work, is in reasonable agreement with the value obtained by the more extensive study reported by Perey.[8]

[9] P. E. Hodgson, Phys. Letters 3, 352 (1963).

In Ref. 8 a correlation was found between W_D and $(N-Z)/A$. For comparison the values of W_D that were obtained from the optical-model analysis of the 11.7-MeV data are plotted as a function of $(N-Z)/A$ in Fig. 6. It is likely that the value obtained for Ni^{58} is influenced by compound-nucleus contributions to the data. The solid line in Fig. 6 represents a straight line least-squares fit to the plotted points with the Ni^{58} point excluded. The slope thus obtained is in fair agreement with the values obtained by Perey from the analysis of 14.3-, 17-, and 22.2-MeV data. The value of W_S for a given value of $(N-Z)/A$ is lower by a few MeV than the values obtained from the analysis of Ref. 8 with the spherically symmetric optical model. It is reasonable to obtain a lower value of W_D in the present strong coupling analysis because one important absorption channel is treated explicitly.

The authors gratefully acknowledge the helpful discussions and comments of F. G. Perey.

PHYSICAL REVIEW VOLUME 133, NUMBER 2B 27 JANUARY 1964

Parity Nonconservation in Nuclei*

F. Curtis Michel†
California Institute of Technology, Pasadena, California
(Received 21 June 1963)

The influence of the known weak interactions on the parity impurity of nuclear states is discussed. Derivation of a parity nonconserving interaction rests on the assumption of a current-current hypothesis for the weak interactions. Consequently, observation of parity impurity effects would be an important confirmation of this hypothesis. A simple approximate method of treating the nuclear parity impurity is developed and applied in an effort to find experimental situations favorable to observation of effects due to such impurity. Parity-forbidden alpha decay from excited states of light nuclei and certain electromagnetic transitions in the heavy nuclei appear to be promising. Special attention has been paid to the internal conversion electrons from the 123-keV transition in Lu^{173} whose polarization is estimated to be about 0.4%. An effect on polarized neutrons analogous to "optical rotation" is also discussed.

I. INTRODUCTION

THE motivation for examining parity nonconservation in nuclei is at least twofold. Firstly, it is desirable to test the parity conservation of all interactions[1] since the weak interactions, such as beta decay, are known not to conserve parity. This program has been largely fulfilled in that experiments[2–19] have already placed exceedingly small upper limits on parity nonconservation in either the electromagnetic or nuclear interactions. If experiment ultimately detects the small deviations to be discussed here, the known parity-

* Supported by the Office of Naval Research.
† Present address: Space Science Department, Rice University, Houston, Texas.
[1] D. H. Wilkinson, Phys. Rev. **109**, 1603 (1958).
[2] N. W. Tanner, Phys. Rev. **107**, 1203 (1957).
[3] R. E. Segel, J. V. Kane, and D. H. Wilkinson, Phil. Mag. **3**, 204 (1958).
[4] D. A. Bromley, H. E. Gove, J. A. Kuehner, A. E. Litherland, and E. Almqvist, Phys. Rev. **114**, 758 (1959).
[5] W. Kaufmann and H. Wäffler, Nucl. Phys. **24**, 62 (1961).
[6] D. E. Alburger, R. E. Pixley, D. H. Wilkinson, and P. Donovan, Phil. Mag. **6**, 171 (1961).
[7] R. E. Segel, J. W. Olness, and E. L. Sprenkel, Phys. Rev. **123**, 1382 (1961).
[8] R. E. Segel, J. W. Olness, and E. L. Sprenkel, Phil. Mag. **6**, 163 (1961).
[9] J. R. Stevens, Ph.D. thesis, California Institute of Technology, 1962 (unpublished).
[10] D. H. Wilkinson, Phys. Rev. **109**, 1614 (1958).
[11] F. Boehm and U. Hauser, Nucl. Phys. **14**, 615 (1959).
[12] R. Haas, L. B. Leipuner, and R. K. Adair, Phys. Rev. **116**, 1221 (1959).
[13] L. Grodzins and F. Genovese, Phys. Rev. **121**, 228 (1961).
[14] D. H. Wilkinson, Phys. Rev. **109**, 1610 (1958).
[15] T. Mayer-Kuckuk, Z. Physik **159**, 369 (1960).
[16] R. L. Garwin, G. Gidal, L. M. Lederman, and M. Weinrich, Phys. Rev. **108**, 1589 (1957).
[17] D. G. Davis, R. C. Hanna, F. F. Heymann, and C. Whitehead, Nuovo Cimento **15**, 641 (1960).
[18] E. Heer, A. Roberts, and J. Tinlot, Phys. Rev. **111**, 645 (1958).
[19] D. P. Jones, P. G. Murphy, and P. L. O'Neill, Proc. Phys. Soc. (London) **72**, 429 (1958).